The role of chiral local field enhancements below the resolution limit of Second Harmonic Generation microscopy

V. K. Valev,[1,*] B. D. Clercq,[2] X. Zheng,[3] D. Denkova,[4] E. J. Osley,[5,6] S. Vandendriessche,[1] A. V. Silhanek,[4] V. Volskiy,[3] P. A. Warburton,[5,6] G. A. E. Vandenbosch,[3] M. Ameloot,[2] V. V. Moshchalkov,[4] and T. Verbiest[1]

[1] *Molecular Electronics and Photonics, INPAC, Katholieke Universiteit Leuven, Celestijnenlaan 200 D, B-3001 Leuven, Belgium*
[2] *University Hasselt and transnational University Limburg, BIOMED, Diepenbeek, Belgium*
[3] *ESAT-TELEMIC, Katholieke Universiteit Leuven, B-3001 Leuven, Belgium*
[4] *Nanoscale Superconductivity and Magnetism & Pulsed Fields Group, INPAC, Katholieke Universiteit Leuven, Celestijnenlaan 200 D, B-3001 Leuven, Belgium*
[5] *London Centre for Nanotechnology, University College London, 17-19 Gordon Street, London, WC1H 0AH, UK*
[6] *Department of Electronic and Electrical Engineering, University College London, Torrington Place, London, WC1E 7JE, UK*
[*] *v.k.valev@fys.kuleuven.be*
www.valev.org

Abstract: While it has been demonstrated that, above its resolution limit, Second Harmonic Generation (SHG) microscopy can map chiral local field enhancements, below that limit, structural defects were found to play a major role. Here we show that, even below the resolution limit, the contributions from chiral local field enhancements to the SHG signal can dominate over those by structural defects. We report highly homogeneous SHG micrographs of star-shaped gold nanostructures, where the SHG circular dichroism effect is clearly visible from virtually every single nanostructure. Most likely, size and geometry determine the dominant contributions to the SHG signal in nanostructured systems.

OCIS codes: (180.4315) Nonlinear Microscopy; (240.4350) Nonlinear optics at surfaces; (160.1585) Chiral media; (160.3918) Metamaterials.

References and links

1. J. B. Pendry, "A chiral route to negative refraction," Science **306**(5700), 1353–1355 (2004).
2. S. Zhang, Y.-S. Park, J. Li, X. Lu, W. Zhang, and X. Zhang, "Negative refractive index in chiral metamaterials," Phys. Rev. Lett. **102**(2), 023901 (2009).
3. E. Plum, J. Zhou, J. Dong, V. A. Fedotov, T. Koschny, C. M. Soukoulis, and N. I. Zheludev, "Metamaterial with negative index due to chirality," Phys. Rev. B **79**(3), 035407 (2009).
4. T. Verbiest, K. Clays, and V. Rodriguez, *Second-Order Nonlinear Optical Characterization Technique* (CRC Press, 2009).
5. V. K. Valev, A. Kirilyuk, F. Dalla Longa, J. Kohlhepp, B. Koopmans, and Th. Rasing, "Observation of periodic oscillations in magnetization-induced second harmonic generation at the Mn/Co interface," Phys. Rev. B **75**(1), 012401 (2007).
6. H. W. K. Tom, T. F. Heinz, and Y. R. Shen, "Second-harmonic reflection from silicon surfaces and its relation to structural symmetry," Phys. Rev. Lett. **51**(21), 1983–1986 (1983).
7. T. Petralli-Mallow, T. M. Wong, J. D. Byers, H. I. Yee, and J. M. Hicks, "Circular dichroism spectroscopy at interfaces: a surface second harmonic generation study," J. Phys. Chem. **97**(7), 1383–1388 (1993).
8. P. Fischer and F. Hache, "Nonlinear optical spectroscopy of chiral molecules," Chirality **17**(8), 421–437 (2005).
9. S. Foerier, I. A. Kolmychek, O. A. Aktsipetrov, T. Verbiest, and V. K. Valev, "Optical second harmonic generation chiral spectroscopy," ChemPhysChem **10**(9-10), 1431–1434 (2009).
10. C. H. Lee, R. K. Chang, and N. Bloembergen, "Nonlinear electroreflectance in silicon and silver," Phys. Rev. Lett. **18**(5), 167–170 (1967).
11. A. Kirilyuk and Th. Rasing, "Magnetization-induced-second-harmonic generation from surfaces and interfaces," J. Opt. Soc. Am. B **22**(1), 148–167 (2005).

#153673 - $15.00 USD Received 31 Aug 2011; revised 5 Oct 2011; accepted 5 Oct 2011; published 20 Dec 2011

12. O. A. Aktsipetrov, T. V. Murzina, E. M. Kim, R. V. Kapra, A. A. Fedyanin, M. Inoue, A. F. Kravets, S. V. Kuznetsova, M. V. Ivanchenko, and V. G. Lifshits, "Magnetization-induced second- and third-harmonic generation in magnetic thin films and nanoparticles," J. Opt. Soc. Am. B **22**(1), 138–147 (2005).
13. V. K. Valev, M. Gruyters, A. Kirilyuk, and Th. Rasing, "Influence of quadratic contributions in magnetization-induced second harmonic generation studies of magnetization reversal," Phys. Status Solidi **242**(15), 3027–3031 (2005) (b).
14. Y. Sheng, A. Best, H.-J. Butt, W. Krolikowski, A. Arie, and K. Koynov, "Three-dimensional ferroelectric domain visualization by Cerenkov-type second harmonic generation," Opt. Express **18**(16), 16539–16545 (2010).
15. V. V. Pavlov, J. Ferré, P. Meyer, G. Tessier, P. Georges, A. Brun, P. Beauvillain, and V. Mathet, "Linear and non-linear magneto-optical studies of Pt/Co/Pt thin films," J. Phys. Condens. Matter **13**(44), 9867–9878 (2001).
16. M. Zavelani-Rossi, M. Celebrano, P. Biagioni, D. Polli, M. Finazzi, L. Duò, G. Cerullo, M. Labardi, M. Allegrini, J. Grand, and P.-M. Adam, "Near-field second-harmonic generation in single gold nanoparticles," Appl. Phys. Lett. **92**(9), 093119 (2008).
17. V. K. Valev, X. Zheng, C. G. Biris, A. V. Silhanek, V. Volskiy, B. De Clercq, O. A. Aktsipetrov, M. Ameloot, N. C. Panoiu, G. A. E. Vandenbosch, and V. V. Moshchalkov, "The Origin of Second Harmonic Generation Hotspots in Chiral Optical Metamaterials," Opt. Mater. Express **1**(1), 36–45 (2011).
18. V. K. Valev, A. V. Silhanek, Y. Jeyaram, D. Denkova, B. De Clercq, V. Petkov, X. Zheng, V. Volskiy, W. Gillijns, G. A. E. Vandenbosch, O. A. Aktsipetrov, M. Ameloot, V. V. Moshchalkov, and T. Verbiest, "Hotspot decorations map plasmonic patterns with the resolution of scanning probe techniques," Phys. Rev. Lett. **106**(22), 226803 (2011).
19. C. Anceau, S. Brasselet, J. Zyss, and P. Gadenne, "Local second-harmonic generation enhancement on gold nanostructures probed by two-photon microscopy," Opt. Lett. **28**(9), 713–715 (2003).
20. P. Schön, N. Bonod, E. Devaux, J. Wenger, H. Rigneault, T. W. Ebbesen, and S. Brasselet, "Enhanced second-harmonic generation from individual metallic nanoapertures," Opt. Lett. **35**(23), 4063–4065 (2010).
21. A. V. Zayats, I. I. Smolyaninov, and C. C. Davis, "Observation of localized plasmonic excitations in thin metal films with near-field second-harmonic microscopy," Opt. Commun. **169**(1-6), 93–96 (1999).
22. O. A. Aktsipetrov, I. M. Baranova, E. D. Mishina, and A. V. Petukhov, "Lightning rod effect in surface-enhanced second-harmonic generation," JETP Lett. **40**, 1012–1015 (1984).
23. Y. Pu, R. Grange, C.-L. Hsieh, and D. Psaltis, "Nonlinear optical properties of core-shell nanocavities for enhanced second-harmonic generation," Phys. Rev. Lett. **104**(20), 207402 (2010).
24. A. Bouhelier, M. Beversluis, A. Hartschuh, and L. Novotny, "Near-field second-harmonic generation induced by local field enhancement," Phys. Rev. Lett. **90**(1), 013903 (2003).
25. W. Fan, S. Zhang, N.-C. Panoiu, A. Abdenour, S. Krishna, R. M. Osgood, Jr., K. J. Malloy, and S. R. J. Brueck, "Second Harmonic Generation from a Nanopatterned Isotropic Nonlinear Material," Nano Lett. **6**(5), 1027–1030 (2006).
26. J. Butet, J. Duboisset, G. Bachelier, I. Russier-Antoine, E. Benichou, C. Jonin, and P.-F. Brevet, "Optical second harmonic generation of single metallic nanoparticles embedded in a homogeneous medium," Nano Lett. **10**(5), 1717–1721 (2010).
27. J. Butet, G. Bachelier, J. Duboisset, F. Bertorelle, I. Russier-Antoine, C. Jonin, E. Benichou, and P.-F. Brevet, "Three-dimensional mapping of single gold nanoparticles embedded in a homogeneous transparent matrix using optical second-harmonic generation," Opt. Express **18**(21), 22314–22323 (2010).
28. S. Kujala, B. K. Canfield, M. Kauranen, Y. Svirko, and J. Turunen, "Multipole interference in the second-harmonic optical radiation from gold nanoparticles," Phys. Rev. Lett. **98**(16), 167403 (2007).
29. V. K. Valev, A. V. Silhanek, N. Verellen, W. Gillijns, P. Van Dorpe, O. A. Aktsipetrov, G. A. Vandenbosch, V. V. Moshchalkov, and T. Verbiest, "Asymmetric optical second-harmonic generation from chiral G-shaped gold nanostructures," Phys. Rev. Lett. **104**(12), 127401 (2010).
30. J. Butet, G. Bachelier, I. Russier-Antoine, C. Jonin, E. Benichou, and P.-F. Brevet, "Interference between selected dipoles and octupoles in the optical second-harmonic generation from spherical gold nanoparticles," Phys. Rev. Lett. **105**(7), 077401 (2010).
31. Y. Zeng and J. V. Moloney, "Volume electric dipole origin of second-harmonic generation from metallic membrane with noncentrosymmetric patterns," Opt. Lett. **34**(18), 2844–2846 (2009).
32. V. K. Valev, N. Smisdom, A. V. Silhanek, B. De Clercq, W. Gillijns, M. Ameloot, V. V. Moshchalkov, and T. Verbiest, "Plasmonic ratchet wheels: switching circular dichroism by arranging chiral nanostructures," Nano Lett. **9**(11), 3945–3948 (2009).
33. A. Benedetti, M. Centini, C. Sibilia, and M. Bertolotti, "Engineering the second harmonic generation pattern from coupled gold nanowires," J. Opt. Soc. Am. B **27**(3), 408–416 (2010).
34. M. Centini, A. Benedetti, C. Sibilia, and M. Bertolotti, "Coupled 2D Ag nano-resonator chains for enhanced and spatially tailored second harmonic generation," Opt. Express **19**(9), 8218–8232 (2011).
35. A. Belardini, M. C. Larciprete, M. Centini, E. Fazio, C. Sibilia, M. Bertolotti, A. Toma, D. Chiappe, and F. Buatier de Mongeot, "Tailored second harmonic generation from self-organized metal nano-wires arrays," Opt. Express **17**(5), 3603–3609 (2009).
36. V. K. Valev, A. V. Silhanek, W. Gillijns, Y. Jeyaram, H. Paddubrouskaya, A. Volodin, C. G. Biris, N. C. Panoiu, B. De Clercq, M. Ameloot, O. A. Aktsipetrov, V. V. Moshchalkov, and T. Verbiest, "Plasmons reveal the direction of magnetization in nickel nanostructures," ACS Nano **5**(1), 91–96 (2011).
37. C. G. Biris and N. C. Panoiu, "Second harmonic generation in metamaterials based on homogeneous centrosymmetric nanowires," Phys. Rev. B **81**(19), 195102 (2010).

#153673 - $15.00 USD Received 31 Aug 2011; revised 5 Oct 2011; accepted 5 Oct 2011; published 20 Dec 2011

38. L. Cao, N. C. Panoiu, R. D. R. Bhat, and R. M. Osgood, Jr., "Surface second-harmonic generation from scattering of surface plasmon polaritons from radially symmetric nanostructures," Phys. Rev. B **79**(23), 235416 (2009).
39. J. I. Dadap, J. Shan, K. B. Eisenthal, and T. F. Heinz, "Second-harmonic Rayleigh scattering from a sphere of centrosymmetric material," Phys. Rev. Lett. **83**(20), 4045–4048 (1999).
40. Y. Zeng, W. Hoyer, J. Liu, S. W. Koch, and J. V. Moloney, "Classical theory for second-harmonic generation from metallic nanoparticles," Phys. Rev. B **79**(23), 235109 (2009).
41. W. L. Schaich, "Second harmonic generation by periodically-structured metal surfaces," Phys. Rev. B **78**(19), 195416 (2008).
42. F. X. Wang, F. J. Rodríguez, W. M. Albers, R. Ahorinta, J. E. Sipe, and M. Kauranen, "Surface and bulk contributions to the second-order nonlinear optical response of a gold film," Phys. Rev. B **80**(23), 233402 (2009).
43. M. J. Huttunen, G. Bautista, M. Decker, S. Linden, M. Wegener, and M. Kauranen, "Nonlinear chiral imaging of subwavelength-sized twisted-cross gold nanodimers," Opt. Mater. Express **1**(1), 46–56 (2011).
44. B. K. Canfield, S. Kujala, K. Laiho, K. Jefimovs, J. Turunen, and M. Kauranen, "Chirality arising from small defects in gold nanoparticle arrays," Opt. Express **14**(2), 950–955 (2006).
45. I. I. Smolyaninov, A. V. Zayats, and C. C. Davis, "Near-field second harmonic generation from a rough metal surface," Phys. Rev. B **56**(15), 9290–9293 (1997).
46. A. V. Zayats, T. Kalkbrenner, V. Sandoghdar, and J. Mlynek, "Second-harmonic generation from individual surface defects under local excitation," Phys. Rev. B **61**(7), 4545–4548 (2000).
47. S. Kujala, B. K. Canfield, M. Kauranen, Y. Svirko, and J. Turunen, "Multipolar analysis of second-harmonic radiation from gold nanoparticles," Opt. Express **16**(22), 17196–17208 (2008).
48. M. Zdanowicz, S. Kujala, H. Husu, and M. Kauranen, "Effective medium multipolar tensor analysis of second-harmonic generation from metal nanoparticles," New J. Phys. **13**(2), 023025 (2011).
49. G. A. E. Vandenbosch, V. Volski, N. Verellen, and V. V. Moshchalkov, "On the use of the method of moments in plasmonic applications," Radio Sci. **46**, RS0E02 (2011).
50. V. K. Valev, A. V. Silhanek, B. De Clercq, W. Gillijns, Y. Jeyaram, X. Zheng, V. Volskiy, O. A. Aktsipetrov, G. A. E. Vandenbosch, M. Ameloot, V. V. Moshchalkov, and T. Verbiest, "U-shaped switches for optical information processing at the nanoscale," Small **7**(18), 2573–2576 (2011).

1. Introduction

It has been almost two centuries since Jean-Baptiste Biot discovered the interaction of chiral materials and polarized light. Since then, this interaction has played a considerably important role in the studies of chemistry, biology and pharmacology. Recently, the prediction [1] and subsequent observation [2,3] of negative refractive index in chiral (meta)materials have triggered a substantial renewal of interest in the interaction between chirality and polarized light. Consequently, optical techniques that are highly sensitive to *chirality*, to (meta)material *(nano)geometries* and to their unusual *electro-magnetic properties* are sought after. As we shall see, the Second Harmonic Generation (SHG) technique fulfills all these conditions and, therefore, understanding the role of individual physical processes that contribute to the SHG signal is of significant importance.

We begin with chirality. The SHG [4] technique exhibits great sensitivity to surfaces and interfaces. For instance, it is capable of monitoring the filling process in a single atomic monolayer during layer-by-layer crystal growth [5]. This sensitivity originates in the fact that, within the dipole approximation, SHG is forbidden in centrosymmetric regions and can only arise from breaks in symmetry. Such breaks in the centrosymmetry include surfaces, interfaces, symmetry of crystalline lattices [6] and, of course, chirality. It has thus been demonstrated that the second harmonic equivalents of optical rotation and circular dichroism are orders of magnitude more sensitive to chirality than their linear counterparts [7–9].

Second, we look at electro-magnetic properties. The SHG process is also highly sensitive to externally applied electric [10] or magnetic [11,12] dc fields; though care should be taken while estimating the latter [13]. When combined with microscopy, SHG can successfully image ferroelectric [14] and ferromagnetic [15] domains, as well as local field enhancements [16–18]. One of the main sources of local field enhancements is attributable to surface plasmon resonances, or "plasmons". Plasmons are coherent oscillations of the charges at the interface between two materials, provided that, within those materials, the real part of the dielectric function changes sign across the interface. For example, gold-air interfaces can support plasmons and those plasmons are readily excitable by the electric field of light. Because SHG scales as the square power of the electric field, it is highly sensitive to plasmons in particular and to local field enhancements in general.

#153673 - $15.00 USD Received 31 Aug 2011; revised 5 Oct 2011; accepted 5 Oct 2011; published 20 Dec 2011

And third, we turn our attention to the nanoscale. Here the sensitivity of SHG presents a double aspect. On the one hand, nanostructures have a very high surface-to-volume ratio; this clearly favors the surface-sensitive SHG. On the other hand, local field enhancements are readily excitable by light in nanostructures, which in turn leads to SHG enhancements. Indeed, such enhancements have been reported from various structural geometries at the nanoscale: nanostructures [19], nanoapertures [20] and pits [21] in metal film, shape singularities [22], core-shell nanocavities [23], etc. These enhancements find a practical application in tip-enhanced SHG scanning near-field microscopy [24], in further enhancing the SHG in nonlinear optical materials, such as GaAs [25] and in the possibility to detect single nanoparticles [26-27]. From the fundamental point of view, the local field enhanced SHG allows the study of contributions to the signal from physical mechanisms that are typically very small, namely multipolar contributions to the SHG [28-30] or electric dipole contributions from the bulk [31]. Additionally, the plasmonic mechanisms themselves, such as coupling between the charge oscillations, can be studied in the SHG enhanced signal [32–35]. Moreover, the enhanced SHG brings insight into new optical and magneto-optical [36] properties, and has lead to the development of several theoretical models [37–42].

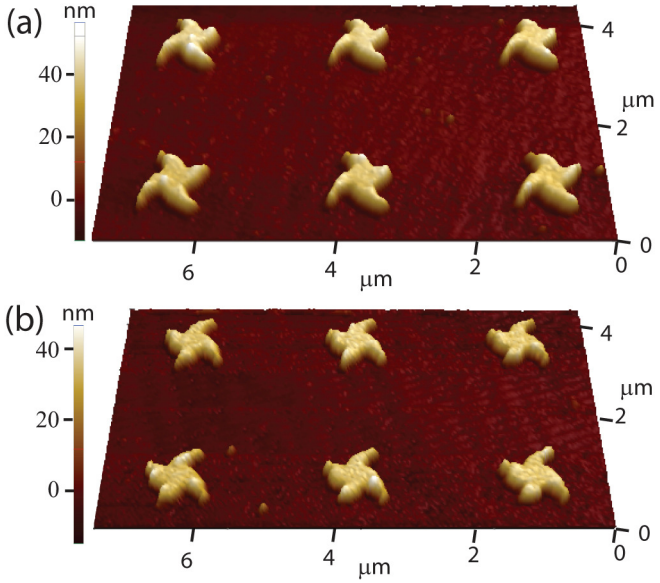

Fig. 1. Atomic force microscopy reveals numerous defects in the fabricated nanostructures. The spiral arms of the stars exhibit discontinuities, variations in size and bumps, for both the right-handed, in (a), and the left-handed, in (b), curved stars.

In the study of chiral metallic nanostructures, we have seen that the SHG signal contains contributions from the chirality, the electro-magnetic properties and the geometry at the nanoscale; it is therefore important to understand which contributions are dominant. Previously, we demonstrated that, for sufficiently large nanostructures (chiral unit cells of 2.4 μm at λ = 800 nm), SHG microscopy is capable of mapping the chirality of the local field enhancements [33]. The contribution from chirality in these results is obviously large and structural defects seem to play a negligible role. Unfortunately, the capability of mapping chiral local field enhancements is lost below the resolution limit of SHG microscopy; where, recently, it has been reported that, in ~300 nm large gold nanodimers at λ = 1060 nm, structural defects play an important role [43]. Structural defects, such as bumps, pits and other small-scale structural deviations [44], are well known sources of SHG enhancement [45,46] and it has been proposed that they contribute through effective higher order multipoles [47,48]. However, between 2.4 μm and 300 nm there is a wide range that remains unexplored. Clearly, the wavelength size is an important limit for physical dimensions and the resolution

#153673 - $15.00 USD Received 31 Aug 2011; revised 5 Oct 2011; accepted 5 Oct 2011; published 20 Dec 2011

limit of the technique is important when it comes to local field enhancements. What are the relative contributions to the SHG signal from defects and from chirality in those regions?

Here, we have studied chiral local field enhancements below the resolution limit of SHG microscopy. We report very *homogeneous* SHG microscopy pictures of chiral gold nanostructures, where the contribution from chirality clearly dominates over that which is attributable to defects. The SHG technique can therefore reliably recognize the handedness of the nanostructures both through the circular dichroism and through absolute intensity measurements. Our measurements are in good agreement with numerical simulations. The precise reasons for the homogeneity of these results will be discussed later. However, we should start by saying that our nanostructures differ both in size and in shape from those that were studied in [32] and [44].

2. Experimental section

Because, at the nanoscale, curves are challenging to fabricate with electron beam lithography, star-shaped gold nanostructures were prepared with curved wedge-shaped arms. Nominally, the structures were 1 μm large and the width of the wedges proceeded from 200 nm to 0 nm. For the preparation, a silicon substrate covered with a thermally grown layer of silicon dioxide, approximately 100 nm, thick was coated with a solution of poly(methyl methacrylate) (PMMA) dissolved in Anisole. The PMMA was then spin-coated on the substrate (2000 RPM, for 45 s and heated to 150 °C for 75 s). Next, patterning of the PMMA layer was produced by electron beam lithography (EBL), followed by resist removal by means of a developer (1 part 4-Methyl-2-pentanone to 3 parts Isopropyl alcohol).

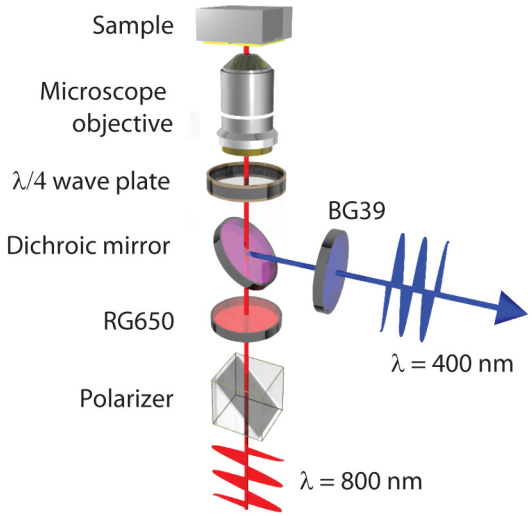

Fig. 2. Schematic diagram of the second harmonic generation microscopy technique in the inverted geometry.

The EBL mask was then placed in a thermal evaporation chamber ($1x10^{-6}$ mBar). An adhesion layer (Cr 5 nm) was evaporated onto the sample using a resistively heated tungsten wire basket, followed by a 35 nm gold layer deposited from a resistively heated molybdenum boat. Finally, lift-off was performed in an acetone bath for several hours, in combination with sonication, in order to remove the unexposed PMMA and its metallic coating leaving behind the metal nanostructures. Because of fabrication defects, the actual structures are less than 800 nm large and the wedge-shaped arms exhibit discontinuities, variations in size and nanobumps, see Figs. 1a and 1b.

A schematic diagram of the SHG microscopy technique in the inverted geometry is shown in Fig. 2. For our measurements, we made use of a commercial Zeiss LSM 510 confocal

#153673 - $15.00 USD Received 31 Aug 2011; revised 5 Oct 2011; accepted 5 Oct 2011; published 20 Dec 2011

microscope. This instrument is a scanning microscope, meaning that the laser spot is scanned at adjustable speed over the sample surface. Consequently, both the intensity of laser light and the scanning velocity offer a degree of control over the laser-induced (over)heating. The illumination is performed with Ti:Sapphire laser pulses, approximately 120 fs long, at a wavelength of 800 nm. The laser light is focused with a x100 objective, NA = 1.46 to a spot of 330 by 440 nm. This spot size is larger than the regions of highest local field enhancements on the nanostructures.

3. Results and discussion

Numerical simulations of the local currents in the nanostructures were calculated with the MAGMAS Maxwell equations solver [49]. This "in house" developed numerical tool has been consistently applied with success to the studies of metal nanostructures [18,36,50]. Figure. 3 shows the local currents at the surface of the star-shaped nanostructures in response to 800 nm excitation light. Figures 3a and 3b correspond to illumination with left- and right-hand circularly polarized light, respectively. More specifically, it can be seen that the strongest enhancements are indicated with four red hotspots in Fig. 3a. These four hotspots form a square with a side of 200 nm. We estimate that the resolution limit in our experiments is larger than 200 nm and that therefore individual hotspots could not be resolved.

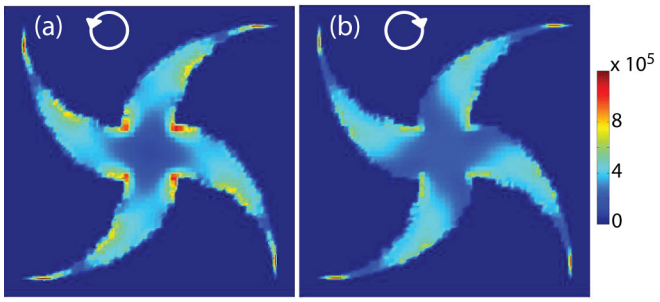

Fig. 3. Numerical simulation of the local currents induced at the surface of the "perfect" nanostructures in response to left-hand, in (a), and right-hand, in (b), circularly polarized light. The direction of rotation for circularly polarized light is indicated with the oriented white circles.

The SHG microscopy pictures from the nanostructures are displayed in Fig. 4, where it is immediately apparent that individual hotspots cannot be resolved. Nevertheless, the sub-resolution limit chiral local field enhancements give rise to a pronounced Second Harmonic Generation – Circular Dichroism (SHG-CD) effect. Namely, there is a clear difference in SHG efficiency for left- (in Fig. 4a) and right- (in Fig. 4b) hand circularly polarized light. Upon reversing the handedness of the nanostructures, this difference in SHG efficiency reverses as well, see Figs. 4c and 4d. It is also immediately apparent that all four panels in Fig. 4 are very homogeneous. There certainly are a few high intensity pixels, but those are more likely attributable to contamination or resist rather than to defects. Indeed these isolated pixels cannot be related to the structural defects at study here because numerous structural defects are present *in all the nanostructures*, as can be seen from Fig. 1 and from the insets in Fig. 4.

#153673 - $15.00 USD Received 31 Aug 2011; revised 5 Oct 2011; accepted 5 Oct 2011; published 20 Dec 2011

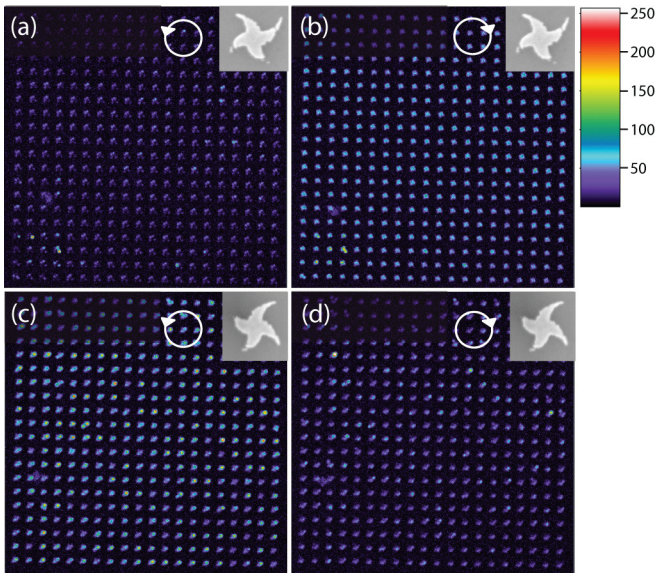

Fig. 4. The Second Harmonic Generation (SHG) is sensitive to chirality and homogenous throughout the arrays. SHG from the right-handed, in (a) and (b), and from the left-handed, in (c) and (d), array of star-shaped nanostructures. SEM micrographs are shown in the insets. The SHG response was recorded for left-hand, in (a) and (c), and right-hand, in (b) and (d), circularly polarized light.

The SHG-CD response was evaluated by subtracting the SHG due to right-hand circularly polarized light from the SHG signal due to left-hand circularly polarized light. This difference is shown for the left-handed and the right-handed nanostructures, in Figs. 5a and 5b, respectively. For the purpose of the calculations, each panel in Fig. 4 has been converted to grayscale and pixel intensities were evaluated. Consequently, the color scale in Fig. 5 corresponds to pixel intensities. Because the SHG-CD is rather small, for clarity, a factor of two has been added to the pixel intensities. It can be seen that both Figs. 5a and 5b are highly homogeneous: every single nanostructure displays the expected sign of circular dichroism. Structural defects, which are mostly situated on the wedge-shaped arms of the stars, contribute as pixels of the "wrong sign", close to the main SHG sources. For a more quantitative comparison, we have evaluated the intensity of each pixel in Figs. 5a and 5b, see Fig. 5c. The average pixel intensity in Figs. 5a and 5b are 131691 and −134845, respectively. Because these values are close to equal and are of opposite sign they are characteristic of "good" circular dichroism response. We find that the contribution that is due to structural defects is significantly smaller than the contribution from chirality. Why is that?

One possible reason is geometry. Indeed, here, the defects are mainly situated on the arms of the stars, while the main local field enhancements occur in the central region. Furthermore, there is size. For instance, it could be that the relative contribution of defects increases with decreasing dimensions of the nanostructures. Additionally, there is the possibility of laser induced damage to the nanostructures during the measurements. In our case, after imaging with left- and right-hand circularly polarized light, the samples were imaged again with left-hand circularly polarized light, to ensure reproducibility. In other words, we explicitly checked that no irreversible changes have occurred during measurement, i.e. the samples were not damaged. We have established that above laser fluence of 2.7 mJ/cm^2, laser damage to individual nanostructures can occur. In practice, we have seen that upon increasing laser intensity or upon slowing the laser spot scanning on the sample surface, individual nanostructures suddenly and irreversibly become much brighter, yielding a very inhomogeneous image.

#153673 - $15.00 USD Received 31 Aug 2011; revised 5 Oct 2011; accepted 5 Oct 2011; published 20 Dec 2011

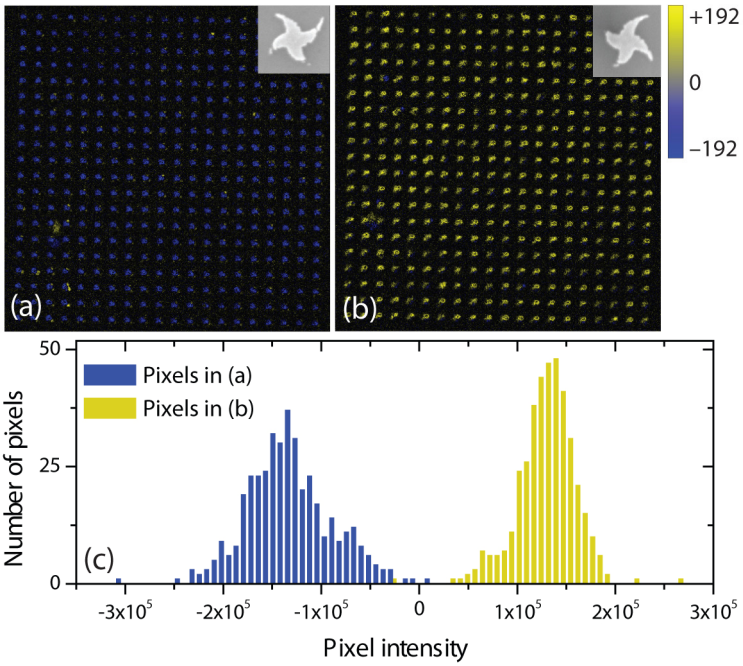

Fig. 5. Second Harmonic Generation – Circular Dichroism from the two arrays of star-shaped gold nanostructures. The SHG signal due to right-hand circular polarization was subtracted from the SHG signal due to left-hand circular polarization, for the left-handed and the right-handed nanostructures, in (a) and (b), respectively. The scale represents the pixel intensity. In (c), a histogram shows all the pixels in (a) and (b) with a given pixel intensity.

In order to understand the reasons why chiral contributions to the SHG signal dominate over the structural ones, we could also look the local field enhancements at the fundamental frequency of a "defective" nanostructure, see Fig. 6.

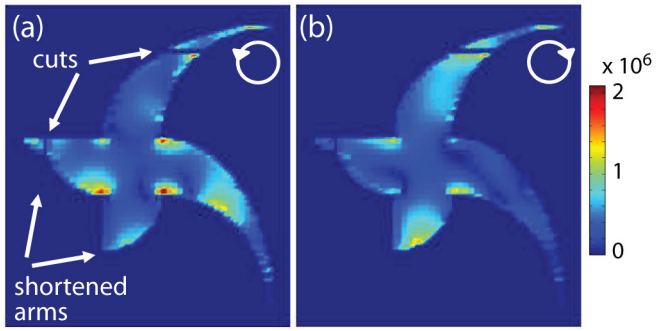

Fig. 6. Numerical simulation of the local currents induced at the surface of the "defective" nanostructures in response to left-hand, in (a), and right-hand, in (b), circularly polarized light. The direction of rotation for circularly polarized light is indicated with the oriented white circles.

We have performed numerical simulations whereby two types of imperfections (or "defects") were introduced – shortened star arms and cuts on the star arms. These simulations show that the local field enhancements, associated with chirality in the "perfect" stars (bright red hotspots), are more intense than local field enhancements resulting from imperfections. It is very tempting to see a confirmation of our SHG results in the local field enhancements simulations. However, caution is required for chirality and defects in metal nanostructures do not necessarily follow the same SHG processes.

#153673 - $15.00 USD Received 31 Aug 2011; revised 5 Oct 2011; accepted 5 Oct 2011; published 20 Dec 2011

4. Conclusions

To summarize, we have applied SHG microscopy to the study of star-shaped gold nanostructures that were made chiral by curved, wedge-shaped arms. According to numerical simulations, even though the size of the nanostructures is comparable to the wavelength of light, the local field enhancements occur below the resolution limit of SHG microscopy. Upon illumination with left- and right-hand circularly polarized light, we obtained very homogeneous SHG micrographs, where the effects of circular dichroism are clearly visible for practically every single nanostructure. Our design confines structural defects to the edges of the star, where their influence on the SHG signal is shown to be smaller than the contributions from the central, chiral, local field enhancements. Our results emphasize the importance of the design, versus simply the scale, of nanostructures with respect to chiral local field enhancements in plasmonic (meta)materials.

Acknowledgments

We acknowledge financial support from the Fund for scientific research Flanders (FWO-V), the K.U. Leuven (GOA), Methusalem Funding by the Flemish government and the Belgian Inter-University Attraction Poles IUAP Programmes. V.K.V., S.V. and A.V.S. are grateful for the support from the FWO-Vlaanderen. B. DC. is thankful to the IWT.

#153673 - $15.00 USD Received 31 Aug 2011; revised 5 Oct 2011; accepted 5 Oct 2011; published 20 Dec 2011